Physica B 673 (2024) 415525

Contents lists available at ScienceDirect

Physica B: Condensed Matter

journal homepage: www.elsevier.com/locate/physb

The structural, morphological and optical studies on $BaAl_2O_4/MgAl_2O_4/MgO$:x% Gd^{3+} ($0 \leq x \leq 1.1$) mixed phases synthesized by sol-gel method

A. Bele [a,*], M.R. Mhlongo [a], L.F. Koao [b], T.E. Motaung [c,d], R.E. Kroon [e], T.T. Hlatshwayo [f], S.V. Motloung [a,g,**]

[a] Department of Physics, Sefako Makgatho Health Sciences University, P. O. Box 94, Medunsa, 0204, South Africa
[b] Department of Physics, University of the Free State (Qwaqwa Campus), Private Bag X 13, Phuthaditjhaba, 9866, South Africa
[c] Department of Chemistry, Sefako Makgatho Health Science University, P. O. Box 65, Medunsa, 0204, South Africa
[d] Department of Chemistry, University of South Africa, P.O. Box 392, UNISA, 0003, South Africa
[e] Department of Physics, University of the Free State, P.O. Box 339, Bloemfontein, 9300, South Africa
[f] Department of Physics, University of Pretoria, Pretoria, 0002, South Africa
[g] Department of Physics and Electronics, Material Science, Innovation and Modelling (MaSIM) Research Focus Area, North-West University (Mafikeng Campus), Mmabatho, South Africa

ARTICLE INFO

Keywords:
Mixed phases
Photoluminescence
Intrinsic defects
Gd^{3+}

ABSTRACT

In this study, $BaAl_2O_4/MgAl_2O_4/MgO$:x% Gd^{3+} (BMM:x% Gd^{3+}) ($0 \leq x \leq 1.1$) mixed phases nanophosphors were prepared for the first-time using sol-gel method. The effect of Gd^{3+} concentration on the morphology, structure, and optical characteristics were examined. X-ray diffraction (XRD) confirmed the presence of hexagonal ($BaAl_2O_4$), cubic ($MgAl_2O_4$ and MgO) phases. Varying the Gd^{3+} concentration has no significant influence on the prepared nanophosphors morphology. Energy dispersive X-ray spectroscopy (EDS) confirmed the presence of the anticipated elementary compositions. Photoluminescence (PL) results showed three emissions peaks located around 312, 616 and 730 nm. The emission peak at 312 nm was ascribed to $^6P_{7/2} \rightarrow {}^6S_{7/2}$ transition in Gd^{3+} whereas other emission peaks originated from other impurities such as Cr^{3+}.

1. Introduction

Rare earth ions (RE^{3+}) doped nanophosphors have emerged as materials with great potential in light emitting diode (LED) manufacturing [1]. Barium aluminate ($BaAl_2O_4$) has different applications and is a light-cumulative fluorescent material with afterglow phosphor properties [2,3]. It has a hexagonal structure with band gap (E_g) of ~3.34 eV [4]. Magnesium aluminate ($MgAl_2O_4$) is another oxide material with various technological applications such as in solid-state lighting and electrical industry [5,6]. It has a face centered cubic (fcc) unit cell with a wide E_g of ~3.20 eV [7,8]. Magnesium oxide (MgO) is said to be an encouraging inorganic material with various applications in water treatment, sensors, and optical coatings [9]. MgO has a cubic structure with E_g of ~4.35 eV [10]. Several synthesis techniques have been adopted in preparation of the various oxide nanophosphor materials [11–15]. In this study, the sol-gel method was used as an alternative synthesis method due to its simplicity compared to other methods [16].

It is reported that rare earths (RE^{3+}) ions doping has an influence on the morphology, particle size, band gap structure and colour tuning of nanocrystals [17,18]. Gd^{3+} ion is one of the RE^{3+} ions most known for the magnetic and good optical behavior [19,20]. Singh et al. [19] reported the luminescence and electron paramagnetic resonance properties of the ultraviolet Gd^{3+} doped $MgAl_2O_4$ phosphors. Two emission peaks were observed at 306 and 312 nm which were respectively attributed to the $^6P_{5/2} \rightarrow {}^8S_{7/2}$ and $^6P_{7/2} \rightarrow {}^8S_{7/2}$ transitions in Gd^{3+}. Singh et al. [20] investigated the luminescence properties of the $BaAl_2O_4$:Gd^{3+} using combustion method and obtained a dominant violet emission at 314 nm which was due to the $^6P_{7/2} \rightarrow {}^8S_{7/2}$ transition of Gd^{3+}. Shehata et al. [21] investigated the effects of Gd^{3+} concentration on the Mgo–$MgAl_2O_4$ nanocomposite synthesized by the co-precipitation method. The XRD results showed that the nanocomposite samples consist of the face-centered cubic structures of both the $MgAl_2O_4$ and MgO. PL results of the undoped and Gd^{3+}-doped nanocomposite showed a green emission in the range of (545–565 nm).

* Corresponding author.
** Corresponding author. Department of Physics, Sefako Makgatho Health Sciences University, P. O. Box 94, Medunsa, 0204, South Africa.
E-mail addresses: abongile.bele@gmail.com (A. Bele), cchataa@gmail.com (S.V. Motloung).

https://doi.org/10.1016/j.physb.2023.415525
Received 26 May 2023; Received in revised form 30 September 2023; Accepted 19 November 2023
Available online 20 November 2023

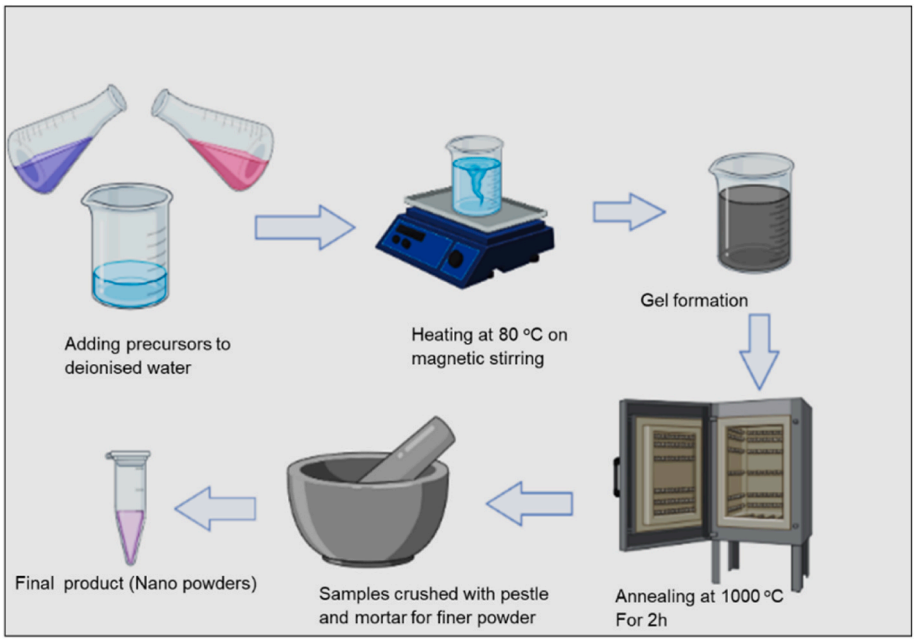

Fig. 1. Schematic diagram of the synthesis of BMM:x% Gd^{3+} ($0 \leq x \leq 1.1$) via sol-gel method.

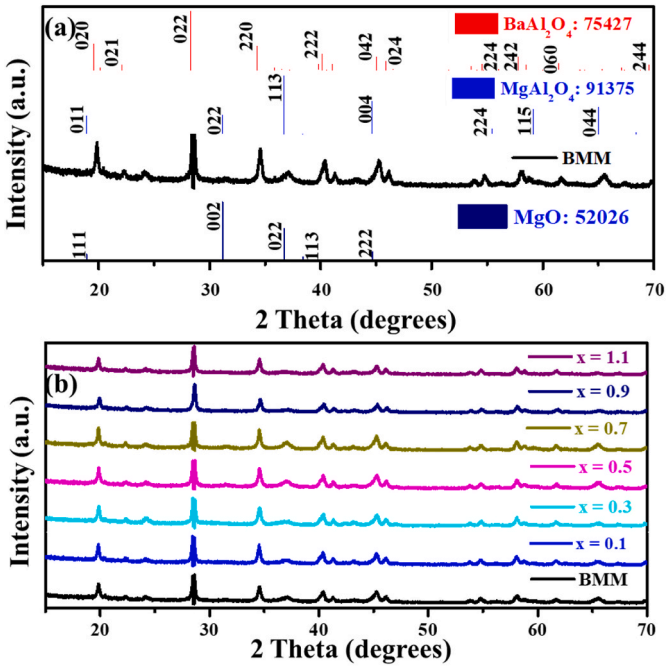

Fig. 2. The X-ray patterns of the (a) BMM and (b) BMM:x% Gd^{3+} ($0 \leq x \leq 1.1$) series.

Table 1
Phase quantification of $BaAl_2O_4$, $MgAl_2O_4$, MgO and $GdAlO_3$.

Sample ID	$BaAl_2O_4$(%)	$MgAl_2O_4$(%)	MgO(%)	$GdAlO_3$(%)
BMM	44.6	50.4	5.00	0.00
x = 0.1	52.4	39.4	5.10	3.10
x = 0.3	57.7	29.7	6.80	5.80
x = 0.5	42.4	53.2	2.20	2.20
x = 0.7	41.7	54.2	2.20	2.00
x = 0.9	62.9	28.2	4.10	4.70
x = 1.1	63.2	26.7	5.40	4.60

Table 2
Estimated crystallite sizes (nm) of the prepared mixed phosphors.

Sample ID	$BaAl_2O_4$ (022)	$MgAl_2O_4$ (113)	MgO (002)
BMM	51	18	49
x = 0.1	39	14	54
x = 0.3	45	22	33
x = 0.5	37	14	59
x = 0.7	44	17	30
x = 0.9	32	13	27
x = 1.1	47	18	32

There are few works that were done on mixed phases [22–24]. With these previous investigations, it is clear that Gd^{3+} has been added as a dopant too in the single phases of both the $MgAl_2O_4$, $BaAl_2O_4$ and nanocomposite of MgO–$MgAl_2O_4$. However, it is emphasized here that BMM mixed phases has not been doped by Gd^{3+}. Thus, this study reports the effects of varying the Gd^{3+} concentration in $BaAl_2O_4$/$MgAl_2O_4$/MgO (BMM) mixed phases with the main aim of producing an alternative material that could potentially be used on the light emitting devices.

2. Experimental

2.1. Sol-gel procedure

The precursors, $Mg(NO_3)_3{\cdot}6H_2O$ (98 %), $Ba(NO_3)_3{\cdot}6H_2O$ (98 %), $Al(NO_3)_3{\cdot}9H_2O$ (98 %), and citric acid (CA) $C_8H_8O_7..H_2O$ (99 %) were dissolved in deionized water to prepare the undoped BMM samples. Various concentrations of $Gd(NO_3)_3{\cdot}6H_2O$ (98 %) were added to the undoped BMM sample to produce doped BMM:x% Gd^{3+} ($0 \leq x \leq 1.1$) nanophosphors. The heating temperature was kept constant at 80 °*C* during the magnetic stirring of the solution. The stirring continued until the gels were formed. After 24 h the gels were annealed in a furnace at 1000 °*C* for 2 h to form a solid product. The solid product was grinded using mortar and pestle to form powder samples. Lastly the fine powders were taken for analysis using different characterization techniques. Fig. 1 shows the summarized version of the procedure followed.

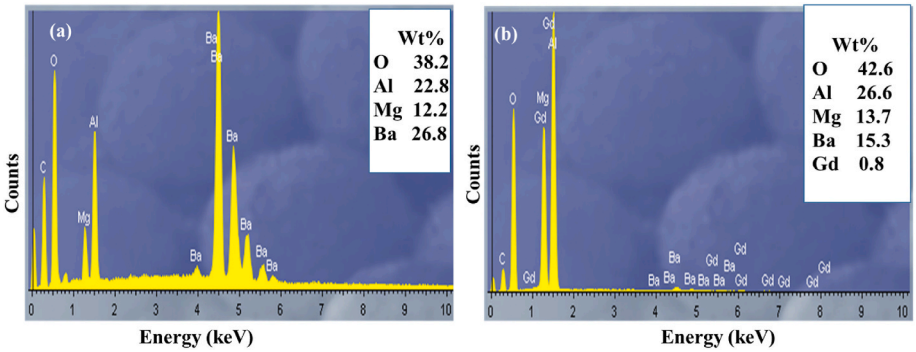

Fig. 3. The EDS spectrum of the (a) BMM sample and (b) x = 0.7 % samples.

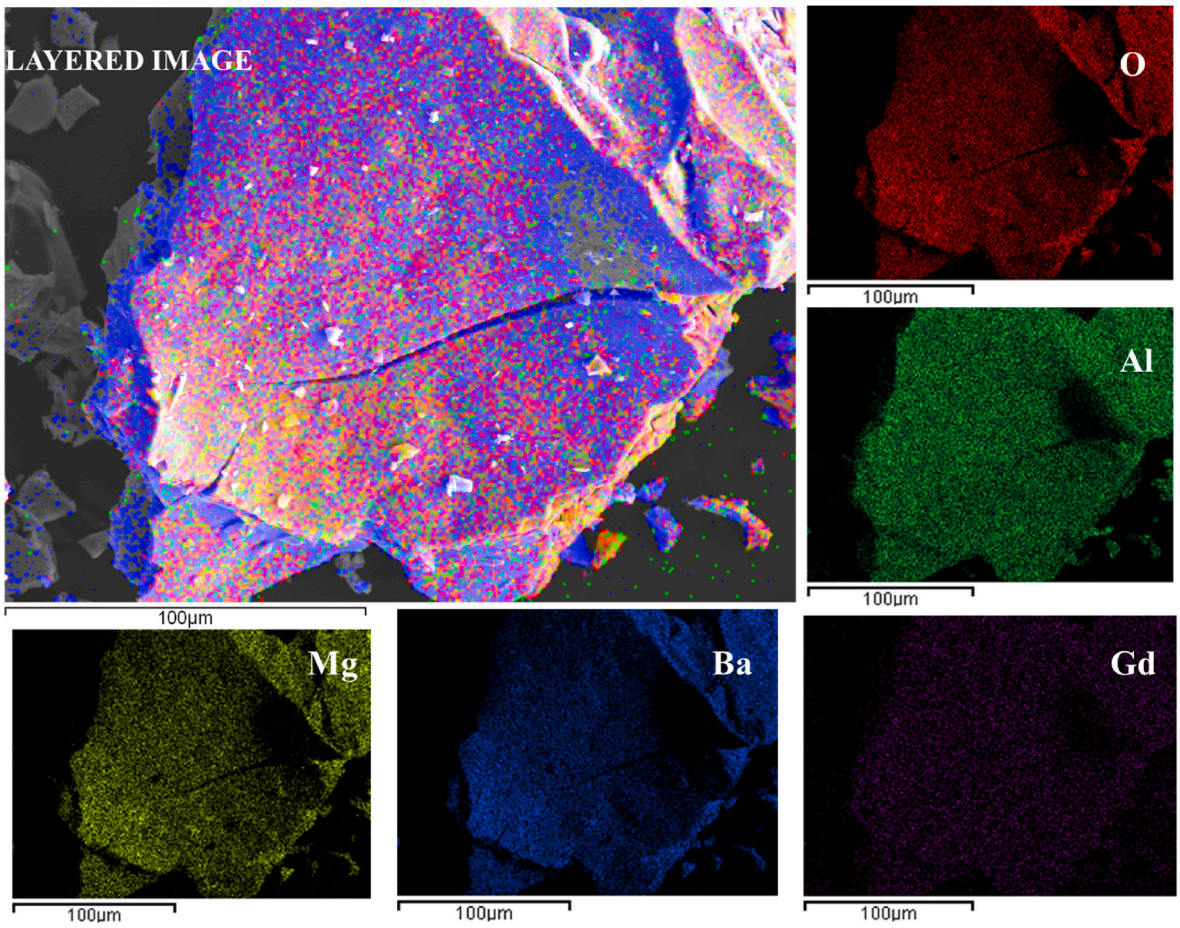

Fig. 4. The EDS elemental map of the x = 0.7 % sample.

2.2. Characterization of BMM nanophosphors

The structural, morphological and chemical composition were investigated using a Bruker D8-Advance powder XRD with a Cu-Kα (1.5405 Å) radiation, Zeiss Supra 55 scanning electron microscope (SEM) in conjunction with energy dispersive X-ray spectroscopy (EDS) and a JEOL JEM 1010 transmission electron microscope (TEM). From XRD scans of the prepared nanophosphors, the phases were identified using X'Pert Highscore Plus software. The relative phase amounts (weight %) was estimated using the Rietveld method. The optical properties were investigated using PerkinElmer Lambda 7505 ultraviolet–visible (UV–vis) spectrophotometer and FLS980 fluorescence spectrophotometer from Edinburgh Instruments.

3. Results and discussion

3.1. Structural, morphological and chemical composition

Fig. 2 (a) shows the XRD pattern for the BMM (undoped) sample. The results indicate that nanophosphors are made up of a mixture of hexagonal ($BaAl_2O_4$, ICSD: 75427), cubic ($MgAl_2O_4$, ICSD: 91375 and MgO, ICSD: 52026). Fig. 2 (b) shows the XRD patterns of the BMM:x% Gd^{3+}($0 \leq x \leq 1.1$) samples with similar diffraction patterns to that of the BMM sample. This indicates that doping has no effect on the crystalline structure of the BMM mixed phases. A similar trend was also observed by Zhang et al. [25] in the study of the structure and luminescence properties of $CaAl_2O_4$ phosphor doped with Sm^{3+}. Table 1 presents the BMM:

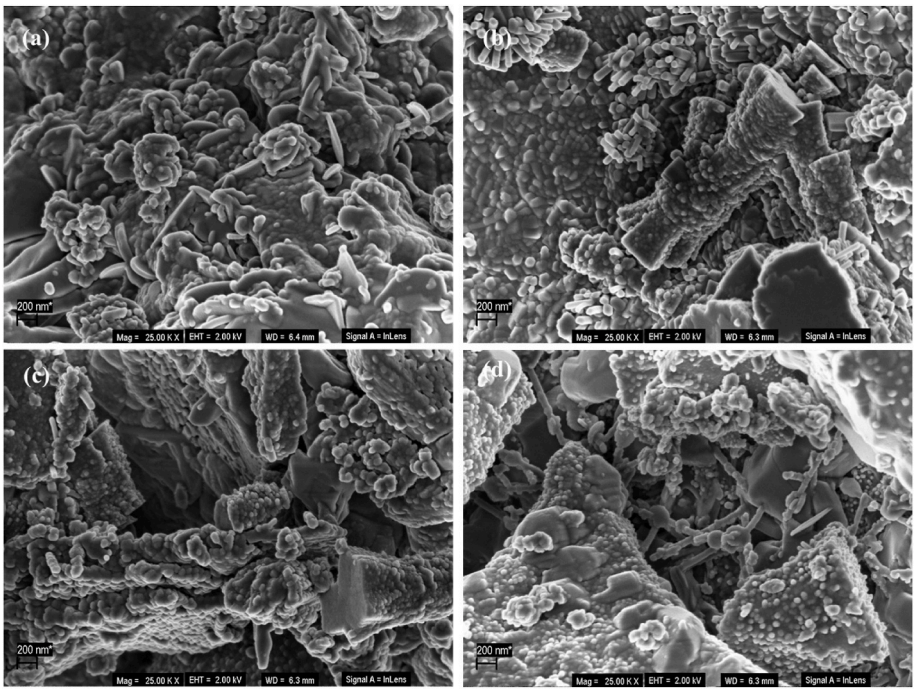

Fig. 5. SEM images of the (a) BMM (b) x = 0.1 % (c) x = 0.7 % and (d) x = 1.1 % samples.

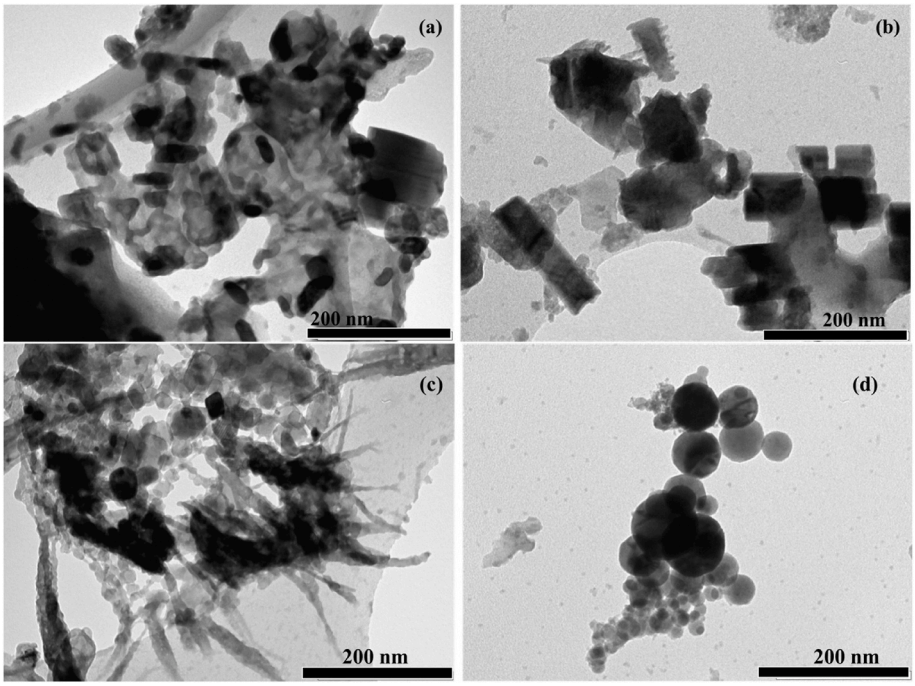

Fig. 6. TEM images of the (a) BMM (b) x = 0.1 (c) 0.7, and (d) 1.1 % samples.

x% Gd^{3+} ($0 \leq x \leq 1.1$) phase quantification results. The results indicate that there is an additional $GdAlO_3$ phase that results from doping with Gd^{3+}. The reason why there is $GdAlO_3$ phase on the doped sample might be due to the chemical affinity between the nitrates of both Gd $(NO_3)_3{\cdot}6H_2O$ and $Al(NO_3)_3{\cdot}9H_2O$ used during synthesis. The quantification results also indicate that in all the samples, $BaAl_2O_4$ and $MgAl_2O_4$ are the major phases contributing to more than 80 % of the samples, while MgO and $GdAlO_3$ are the minor phases. The crystallite sizes were estimated using the Scherrer equation [26] by using the most intense diffraction peak of each individual phase present in BMM and the results are presented in Table 2. The results showed that the crystallite sizes fluctuate with an increase in Gd^{3+} concentration. Thus, the crystallite size is influenced by the Gd^{3+} concentration.

Elemental analysis was performed by the EDS. Fig. 3 (a) shows the EDS spectra of the BMM, which confirms the presence of the Ba, Mg, Al, and O. Fig. 3 (b) shows with the x = 0.7 % Gd^{3+} which confirms the presence of additional Gd in comparison to the BMM sample. The carbon (C) peak in Fig. 3 (a) and (b) are due to carbon being used as a coating material during the sample preparation for SEM analysis. Fig. 4 shows the elementary map for the x = 0.7 % sample and the results confirmed

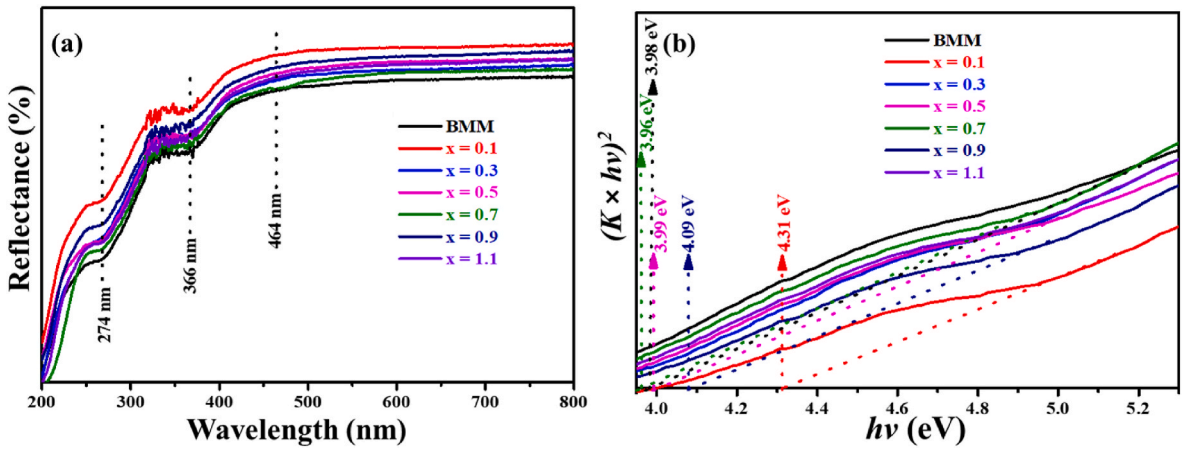

Fig. 7. (a) The diffuse reflectance spectra of BMM:x% Gd^{3+} ($0 \leq x \leq 1.1$) (b) Tauc of BMM: x% Gd^{3+} ($0 \leq x \leq 1.1$).

Table 3
Estimated E_g of the selected samples.

Sample ID	BMM	x = 0.1	x = 0.5	x = 0.7	x = 0.9
E_g (eV)	3.98	4.31	3.99	3.96	4.09

the distribution of elementary composition all over the surface.

The morphological aspects were further investigated by SEM and the images for selected samples are shown in Fig. 5. The results of BMM sample in Fig. 5 (a) reveal the agglomerated non-homogeneous mixture of some scattered nano-rod structures and irregular particles. Fig. 5 (b)–(d) shows morphology for the samples doped with the x = 0.1, 0.7 and 1.1 %, respectively. The sample doped x = 0.1 % showed a mixture of irregular particles with nano-rods. Similar morphology is observed for the other samples. Generally, doping with Gd^{3+} did not show significant

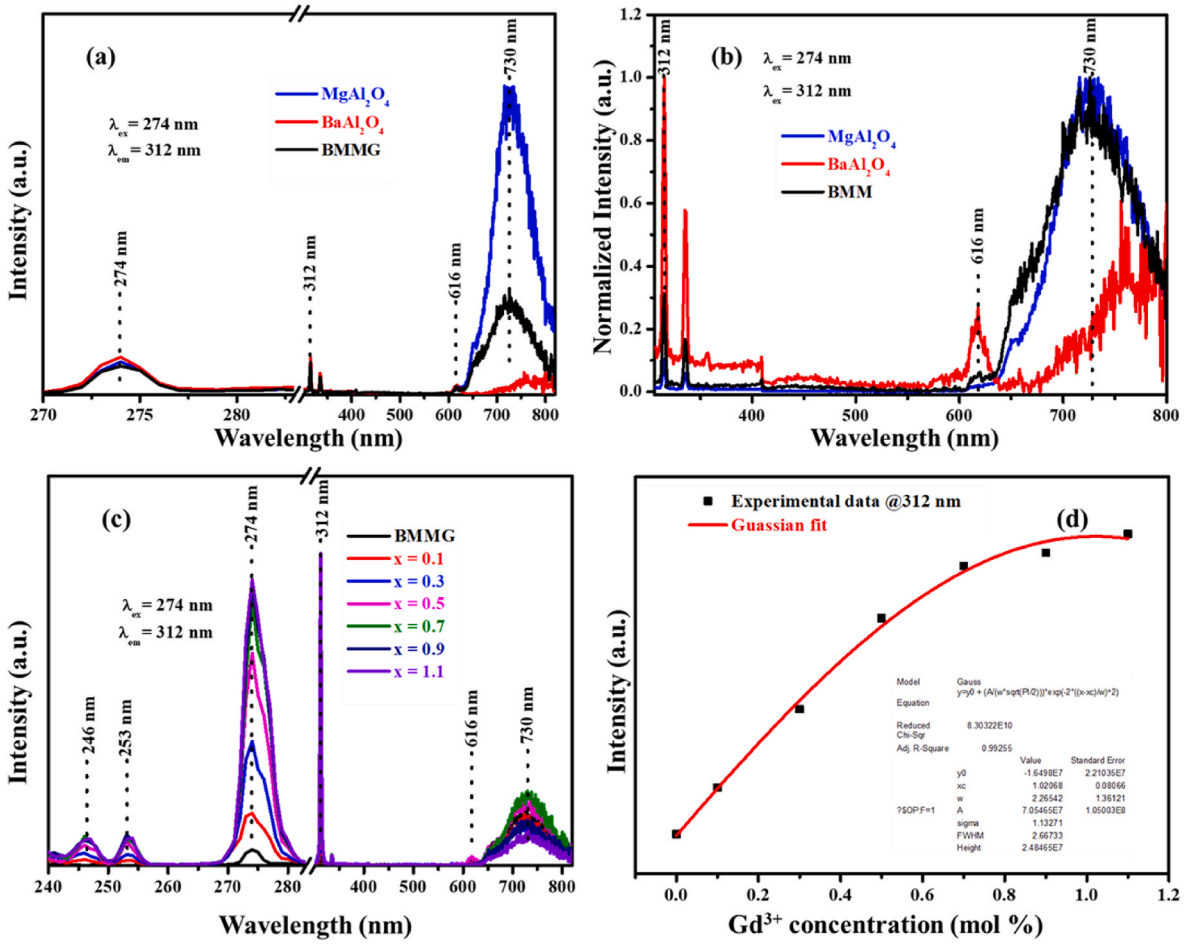

Fig. 8. (a) Emission spectrum of undoped samples ($MgAl_2O_4$, $BaAl_2O_4$, and BMM), (b) normalized spectra of the Fig (a), (c) excitation and emission spectrum of the BMM:x% Gd^{3+} ($0 \leq x \leq 1.1$) and (d) emission intensity at 312 nm as a function of Gd^{3+} concentration.

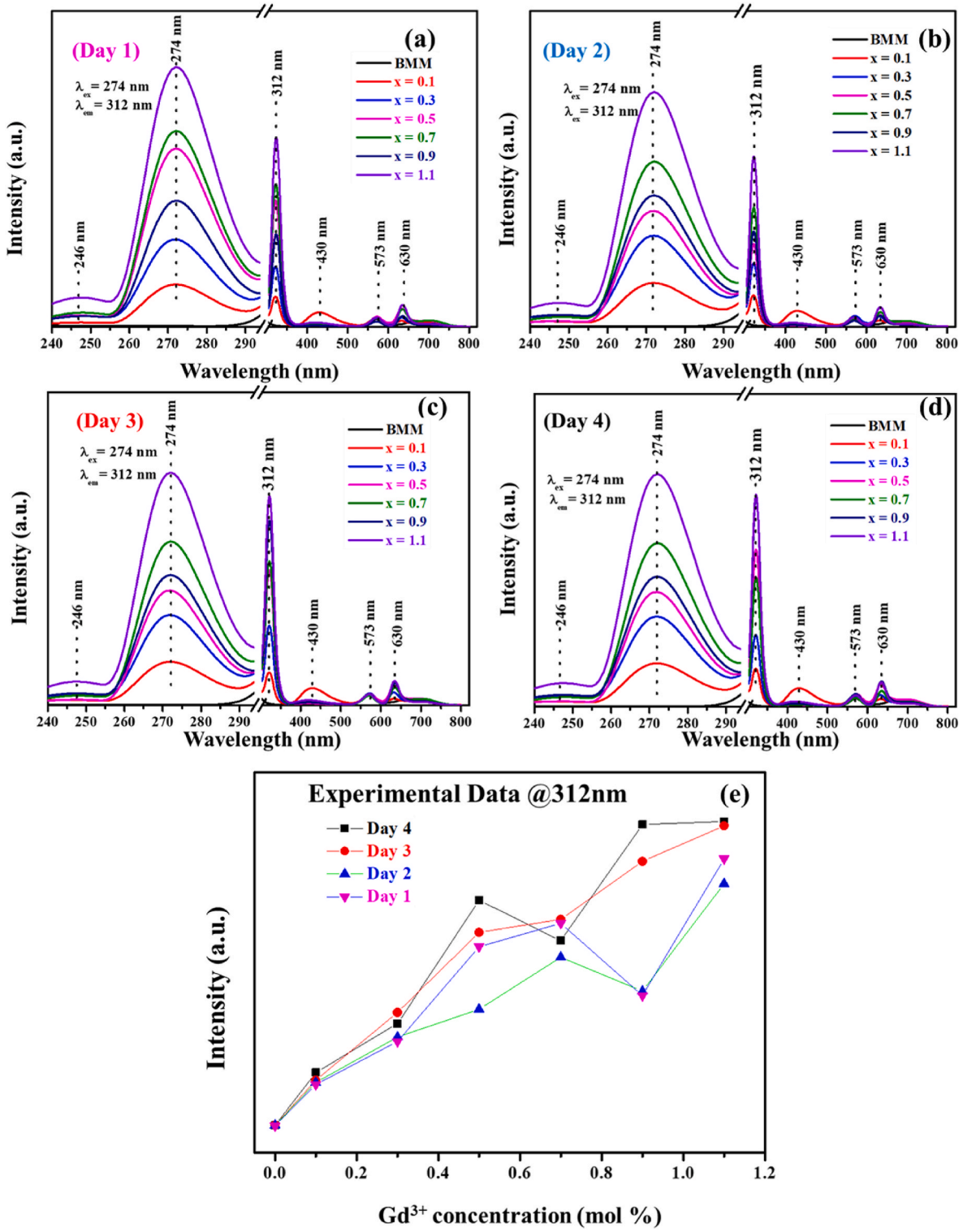

Fig. 9. The PL intensity of the BMM:x% Gd^{3+} ($0 \leq x \leq 1.1$) samples as a function of time over (a) 1 day, (b) 2, (c) 3, (d) 4 days, and emission intensity at 312 nm as a function of Gd^{3+} concentration for different days.

change in morphology.

Furthermore, the selected samples were analyzed with TEM. Fig. 6 (a) shows the image for the BMM and the results reveal that the samples contain an agglomerate and scattered irregular rod-like structures. The sample doped at x = 0.1 and 0.7 % sample in Fig. 6 (b)–(c) show scattered thick rod-like structures like the BMM sample. However, it is noted that for the x = 0.7 % there are development of the spherical particles. The spherical like particle are clearly more pronounced at x = 1.1 % in Fig. 6 (d).

3.2. Optical properties

3.2.1. Uv–vis analysis

Fig. 7 (a) shows the diffuse reflectance spectra of BMM:x% Gd^{3+} ($0 \leq$

$x \leq 1.1$). The findings showed absorption bands at 274, 366 and 464 nm. The absorption band at 274 nm is ascribed to the $O^{2-} \rightarrow Al^{3+}$ charge transition within the $BaAl_2O_4$ of the prepared material [27]. This charge transition arises from electrons that are excited from the valence bandgap energy of O to the conduction bandgap energy of Al [27]. Note that Gd^{3+} ions have a narrow absorption band near 275 nm due to their $^6I_J \leftarrow {}^8S_{7/2}$ transition [28], but here the absorption band at 274 nm occurs even when the Gd^{3+} doping is low or absent, so the observed absorption is not due to the Gd^{3+} ions. The absorption band at around 366 nm is attributed to the defects absorption within $MgAl_2O_4$ [29] while the absorption band located at 464 nm is assigned to the defects absorption within $BaAl_2O_4$ [27]. The results indicate that varying the Gd^{3+} concentration results in the shift in the absorption edges to lower wavelengths compared to BMM even though there is fluctuation. To convert the reflectance R (%) to values proportional to the absorbance and the Tauc plot of $(Khv)^n$, the Kubelka-Munk function $K = (1\text{-}R)^2/(2R)$ [30] was used and plotted versus incident photon energy (hv) as shown in Fig. 7 (b). The E_g were determined by extrapolation of the linear region of the plot $(Khv)^2 = 0$, where $n = 2$ because of that $BaAl_2O_4$, $MgAl_2O_4$, MgO being direct band gaps [4,8,10]. These results show a fluctuation in the band gap as the concentration of Gd^{3+} is increased. This might be due to the fluctuation in crystallite sizes of the phases present in BMM as shown in Table 2. This is motivated by Singh et al. [31] suggestion that the band gap of materials depends on the crystallite sizes of the materials. Table 3 shows the extrapolated E_g. These estimated Eg are close to the theoretical band gap of $BaAl_2O_4$ (3.34 eV) [4], $MgAl_2O_4$ (3.20 eV) [8] and MgO (4.35 eV) [10]. The increase in E_g is due to the to the increase in carrier concentration known as Burstein-Moss (BM) effect [32].

3.2.2. PL analysis

Fig. 8 shows the PL spectra for excitation and emission for the BMM and BMM:x% Gd^{3+} ($0 \leq x \leq 1.1$) samples. Fig. 8 (a) shows the results for undoped BMM samples. The excitation was first monitored at 730 nm emission wavelength; however, no excitation peaks were detected. The emission was then monitored at 312 nm, the results showed a narrow excitation peak at 274 nm. This peak is assigned to the excitation peak of Gd^{3+} due to the $^6I_J \leftarrow {}^8S_{7/2}$ transition of Gd^{3+} [20]. The BMM samples were then excited by 274 nm, emission peaks were observed at 312, 616, and 730 nm as illustrated in Fig. 8 (a). Fig. 8 (b) shows the normalized spectra for the BMM samples, the results confirmed the emission peaks as shown in Fig. 8 (a). The narrow emission at 312 nm is assigned to Gd^{3+} ($^6P_{7/2} \rightarrow {}^8S_{7/2}$ transition) [22] and the narrow emission band at 616 nm might be due to Eu^{3+} ($^5D_0 \rightarrow {}^7F_2$) transition) contamination [33]. Lastly, we propose that the broad emission at 730 nm be assigned to Cr^{3+} present as an impurity in Al [34]. Fig. 8 (c) illustrates the excitation and emission spectra for the BMM:x% Gd^{3+} ($0 \leq x \leq 1.1$) samples. The results show absorption peaks at 246, 253, 274 and 276 nm, these peaks relate to the f-f transitions of Gd^{3+} and are attributed to the transitions of $^8S_{7/2} \rightarrow {}^6D_{7/2}$, $^8S_{7/2} \rightarrow {}^6D_{9/2}$, $^8S_{7/2} \rightarrow {}^6I_{15/2}$ and $^8S_{7/2} \rightarrow {}^6I_{9/2}$, respectively [20]. The results also revealed the emission peaks at 312, 616, and 730 nm. The emission peak at 312 nm was assigned to $^6P_{7/2} \rightarrow {}^8S_{7/2}$ transition of Gd^{3+} [22]. The peak at 616 nm was attributed to be maybe a Eu^{3+} contamination [33]. Fig. 8 (d) shows the emission intensity as a function of Gd^{3+} concentration. The results show an increase in 312 nm emission intensity with an increase in Gd^{3+} concentration which was fitted using the Gaussian fit. The intensity increases with an increasing concentration of Gd^{3+}. The observed increase is attributed to the phenomenon of the luminescence enhancement that is associated with Gd^{3+} doping [35].

Fig. 9 (a)-(d) shows the PL intensity as a function of time over the days for the BMM:x% Gd^{3+} ($0 \leq x \leq 1.1$) samples. The emission wavelength was monitored at 312 nm and two excitation wavelengths at 246 and 274 nm were observed. These excitations were also observed in Fig. 8 and were attributed to Gd^{3+} transitions. All samples were then excited with 274 nm and emission peaks at 312, 430, 573 and 630 nm were observed. The peaks at 430, 573 and 630 nm were not observed in Fig. 8 and this may be due to material (powder) handling. Lovén et al. [36] suggested that powder handling generates high emissions. These peaks are assigned to the intrinsic defects within $BaAl_2O_4$ such as oxygen vacancies (V_O) and Ba vacancies (V_{Ba}) [37]. Fig. 9 (e) shows the emission intensity at 312 nm as a function of Gd^{3+} concentration for different days. The results show an increase in luminescence intensity with an increase in Gd^{3+} concentration. The luminescence intensity also varies with days and this is attributed to the material degradation. This is motivated by Peng et al. [38] suggestion that luminescence intensity depends on material degradation.

4. Conclusion

The citrate sol-gel method was used to successfully prepare BMM:x% Gd^{3+}($0 \leq x \leq 1.1$) nanophosphors. The structural, morphological and optical studies were performed on the prepared BMM: x% Gd^{3+} ($0 \leq x \leq 1.1$) mixed phases nanophosphors. XRD results indicated that the material consists of hexagonal ($BaAl_2O_4$) and cubic ($MgAl_2O_4$ and MgO) mixed phases. SEM results showed a slight change in morphology of the samples with an addition of Gd^{3+}. All the anticipated elements were confirmed using the EDS. TEM results demonstrated that the particle morphology is affected by varying the Gd^{3+} concentration. The UV–vis results suggested that the E_g values depend on the Gd^{3+} concentration. PL results showed excitation and emission peaks assigned f-f transitions of Gd^{3+}. PL results as a function of time over days showed evidence of material degradation.

Credit author statement

A. Bele: Conceived and designed the experiments; Performed the experiments; Analyzed and interpreted the data; Contributed reagents, materials, analysis tools or data; Wrote the paper. **M.R. Mhlongo**, **L.F. Koao**: Conceived and designed the experiments; Analyzed and interpreted the data; Contributed reagents, materials, analysis tools or data. **T.E. Motaung**, **R.E. Kroon**, **T.T. Hlatshwayo**: Analyzed and interpreted the data; Contributed reagents, materials, analysistools or data. **S.V. Motloung**: Conceived and designed the experiments; Analyzed and interpreted the data; Contributed reagents, materials, analysis tools or data; Wrote the paper.

Declaration of competing interest

The authors declare that they have no known competing financial interests or personal relationships that could have appeared to influence the work reported in this paper.

Data availability

Data will be made available on request.

Acknowledgements

This work is supported by the South African National Research Foundation (NRF) Thuthuka programme (fund number: UID 13947), NRF incentive funding for rated researchers (IPRR) (Grant No: 114924), SMU Physics department research fund and SMU Electron Microscope Unit.

References

[1] W. Li, N. Ma, B. Devakumar, X. Huang, Blue-light-excitable broadband yellow-emitting $CaGd_2HfSc(AlO_4)_3:Ce^{3+}$ garnet phosphors for white light-emitting diode devices with improved color rendering index, Mater. Today 23 (2022), 100638.

[2] Y. Ishii, H. Tsukasaki, S. Kawaguchi, Y. Ouchi, S. Mori, Structural investigation of the $SrAl_2O_4$-$BaAl_2O_4$ solid solution system with unstable domain walls, J. Comm. Mat. 249 (2017) 149.

[3] V. Singh, V. Natarajan, J.J. Zhu, Photoluminescence, thermoluminescence and electron spin resonance studies on Eu^{3+} doped $Ca_3Al_2O_6$ red phosphors, Opt. Mater. 29 (2007) 1447.

[4] A. Salehabadi, M. Salavati-Niasari, F. Sarrami, A. Kartonb, Sol-Gel auto-combustion synthesis and physicochemical properties of $BaAl_2O_4$ nanoparticles; electrochemical hydrogen storage performance and density functional theory, Renew. Energy 114 (2017) 1419.

[5] S.M. Ahmad, T. Hussain, Riaz Ahmad, J. Siddiqui, D. Ali, Synthesis and characterization of magnesium aluminate ($MgAl_2O_4$) spinel (MAS) thin films, Mater. Res. Express 5 (2018), 016415.

[6] F. Zhang, S.S. Wong, Ambient large-scale template-mediated synthesis of high-aspect ratio single-crystalline, chemically doped rare-earth phosphate nanowires for bioimaging, ACS Nano 4 (2010) 99.

[7] J. Lin, Y. Haung, J. Zhang, F. Shi, S. Wei, J. Gao, X. Ding, C. Tang, Synthesis and photoluminescence properties of $MgAl_2O_4$:Mn^{2+} hexagonal nanoplates, Mater. Res. Bull. 44 (2009) 106–109.

[8] M.Z. Salmasi, M. Kazemeini, S. Sadjadi, R. Nematollahi, Spinel $MgAl_2O_4$ nanospheres coupled with modified graphitic carbon nitride nanosheets as an efficient Z-scheme photocatalyst for photodegradation of organic, contaminantsApp, Surf. Sci. 585 (2022), 152615.

[9] G. Balakrishnan, R. Velavan, K.M. Batoo b, E.H. Raslan, Microstructure, optical and photocatalytic properties of MgO nanoparticles, Results Phys. 16 (2020), 103013.

[10] L. Sohrabi, F. Taleshi, R. Sohrabi, Effect of carbon nanotubes support on band gap energy of MgO nanoparticles, J. Mater. Sci. Mater. Electron. 25 (2014) 4110.

[11] M. Freeda, T.D. Subash, Photoluminescence studies of Terbium doped Calcium Aluminate nanophosphors ($CaAl_2O_4$:Tb) synthesized by sol-gel method, Mater. Today 4 (2017) 4283.

[12] X. Yuan, Y.B. Xu, Y.Y. He, Synthesis of $Ca_3Al_2O_6$ via citric acid precursor, Mat. Sci. Eng. A-Struct. Mater. Prop. Micro. Proc. 447 (2007) 142.

[13] E.N. Alvar, M. Rezai, H.N. Alvar, Synthesis of nanocrystalline $MgAl_2O_4$ spinel by using ethylene diamine as precipitation agent, Synth. Pow. Tech. 2 (2010) 268.

[14] M.M. Abbas, M. Rasheed, Solid state reaction synthesis and characterization of Cu doped TiO_2 nanomaterials, J. Phys.: Conf. Ser. 1795 (2021), 012059.

[15] S.T. Aruna, A.S. Mukasyan, Combustion synthesis and nanomaterials, Cur. Opi. In Sol. Sta. and Mat. Sci. 12 (2008) 44.

[16] Z. Zhu, X. Li, Q. Zhao, S. Liu, X. Hu, G. Chen, Facile solution synthesis and characterization of porous cubic-shaped superstructure of $ZnAl_2O_4$, Mater. Lett. 65 (2011) 194.

[17] A.H. Wako, F.B. Dejene, H. C Swart, Combustion synthesis, characterization and luminescence properties of barium aluminate phosphor, J. Rare Earths 32 (2014) 806.

[18] V. Kumar, S. Som, V. Kumar, V. Kumar, O.M. Ntwaeaborwa, E. Coetsee, H.C. Swart, Tunable and white emission from ZnO: Tb^{3+} nanophosphors for solid state lighting applications, J. Chem. Eng. 255 (2014) 541–552.

[19] V. Singh, G. Sivaramaiah, J.L. Rao, S.H. Kim, Luminescence and electron paramagnetic resonance investigation on ultraviolet emitting Gd doped $MgAl_2O_4$ phosphors, J. Lumin. 143 (2013) 1162.

[20] V. Singh, G. Sivaramaiah, N. Singh, M.S. Pathak, J.L. Rao, P.K. Singh, A.S. Nagpure, Ultraviolet B emission from a Gd^{3+}-doped $BaAl_2O_4$ powder phosphor, Bull. Mater. Sci. 42 (2019) 19.

[21] M.M. Shehata, S.A. Waly, Y.A. Abdelaziz, Effect of Gd3+ doping on structural and optical properties of MgO–MgAl2O4 nanocomposites synthesized via co-precipitation method, J. Mater. Sci. Mater. Electron. 32 (2021) 7423.

[22] M.R. Mhlongo, L.F. Koao, R.E. Kroom, T.E. Motaung, S.V. Motloung, Effects of annealing period on the structure and photoluminescence of the mixed phases $ZnAl_2O_4/ZnO/SrAl_2O_4/Sr_3Al_2O_6$:0.025% Tb^{3+} nanophosphor synthesized by sol-gel techinique, J. Mol. Struct. 1184 (2019) 92.

[23] L.T. Melato, O.M. Ntwaeaborwa, R.E. Kroon, T.E. Motaung, S.V. Motloung, Effect of Ho^{3+} concentration on the structure, morphology and optical properties of $Ba_{0.5}Mg_{0.5}Al_2O_4$ nanophosphor, J. Mol. Struct. 1176 (2019) 217.

[24] Z. Wang, P. Li, Q. Guo, Z. Yang, A single-phased warm white-light-emitting phosphor $BaMg_2(PO_4)_2$:Eu^{2+}, Mn^{2+}, Tb^{3+} for white light emitting diodes, Mater. Res. Bull. 52 (2014) 30.

[25] X. Zhang, H. Dong, Z. Mei, Structure and luminescence properties of Sm^{3+} doped in $CaAl_2O_4$ phosphor, Optoelectron, Adv. Mater. Rapid Commun. 4 (2010) 28.

[26] D. Jia, X.J. Wang, E. van der Kolk, W.M. Yen, Electron traps in Tb^{3+}-doped $CaAl_2O_4$, Opt Commun. 204 (2002) 247.

[27] V. Maphiri, M.R. Mhlongo, T.T. Hlatshwayo, T.E. Motaung, L.F. Koao, S. V. Motloung, Citrate sol-gel synthesis of $BaAl_2O_4$:x% Cu^{2+} ($0 \leq x \leq 1$) nano-phosphors: structural, morphological and photoluminescence properties, Opt. Mater. 109 (2020), 110244.

[28] M.H.M. Abdelrehman, R.E. Kroon, A. Yousif, H.A.A.S. Ahmed, H.C. Swart, Photoluminescence, thermoluminescence, and cathodoluminescence of optimized cubic Gd_2O_3:Bi phosphor powder, J. Vac. Sci. Technol. 38 (2020) 3207.

[29] A. Lushchika, S. Dolgova, E. Feldbacha, R. Parejab, A.I. Popovc, E. Shablonina, V. Seemana, Creation and thermal annealing of structural defects in neutron-irradiated $MgAl_2O_4$ single crystals, Nucl. Instrum. Methods Phys. Res. B (2017) 1.

[30] S.-F. Wang, G.-Z. Sun, L.-M. Fang, L. Lei, X. Xiang, X.-T. Zu, A comparative study of $ZnAl_2O_4$ nanoparticles synthesized from different aluminium salts for use as fluorescence materials, Sci. Rep. 5 (2015), 12849.

[31] M. Singh, M. Goyal, K. Devlal, Size and shape effects on the band gap of semiconductor compound nanomaterials, J. Taibah Univ. Sci. 12 (2018) 470.

[32] N. Narayanana, N.K. Deepak, Ga dopant induced band gap broadening and conductivity enhancement in spray pyrolysed $Zn_{0.85}Ca_{0.15}O$ thin films, Mat. Res. 21 (2018), 20180034.

[33] D. den Engelsen, P. Harris, T. Ireland, J. Silver, Cathodoluminescence of nanocrystalline Y_2O_3:Eu^{3+} with various Eu^{3+} concentrations, J. Solid State Sci. Technol. 4 (2015) R1.

[34] J. Zhoua, Z. Xia, Synthesis and near-infrared luminescence of $La_3GaGe_5O_{16}$:Cr^{3+} phosphors, RSC Adv. 4 (2014), 46313.

[35] L. Stagi, D. Chiriu, A. Ardu, C. Cannas, C.M. Carbonaro, P.C. Ricci, Luminescence enhancement by energy transfer in melamine-Y_2O_3:Tb^{3+} nanohybrids, J. Appl. Phys. 118 (2015), 125502.

[36] K. Lovén, Sara, M. Franzén, C. Isaxon, M.E. Messing, J. Martinsson, A. Gudmundsson, J. Pagels, M. Hedmer, N. Lund, Emissions and exposures of graphene nanomaterials, titanium dioxide nanofibers, and nanoparticles during down-stream industrial handling, J. Expo. Sci. Environ. Epidemiol. 31 (2021) 736.

[[3][7]] D. D Engelsen, G.R. Fern, T.G. Ireland, F. Yang, J. Silver, Photoluminescence and cathodoluminescence of $BaAl_2O_4$:Eu^{2+} and undoped $BaAl_2O_4$: evidence for F-centres, Opt. Mater. Express 10 (2020) 1962.

[38] W. Peng, H. Xia, Z. Zhang, T. Qi, S. Kong, W. Dai, Z. Huang, A surface corrosion and expansion mechanism on thermal degradation of $SrAl_2O_4$:Eu^{2+}, Dy^{3+}, J. of All. and Comp. 753 (2018) 35.